

Three-Dimensional *In Vivo* Imaging of the Murine Liver: A Micro-Computed Tomography-Based Anatomical Study

Teresa Fiebig¹, Hanne Boll¹, Giovanna Figueiredo¹, Hans Ulrich Kerl¹, Stefanie Nittka², Christoph Groden¹, Martin Kramer³, Marc A. Brockmann^{1*}

1 Department of Neuroradiology, Medical Faculty Mannheim, University of Heidelberg, Mannheim, Germany, **2** Department of Clinical Chemistry, Medical Faculty Mannheim, University of Heidelberg, Mannheim, Germany, **3** Department of Veterinary Clinical Sciences, Small Animal Clinic, Justus-Liebig-University, Giessen, Germany

Abstract

Various murine models are currently used to study acute and chronic pathological processes of the liver, and the efficacy of novel therapeutic regimens. The increasing availability of high-resolution small animal imaging modalities presents researchers with the opportunity to precisely identify and describe pathological processes of the liver. To meet the demands, the objective of this study was to provide a three-dimensional illustration of the macroscopic anatomical location of the murine liver lobes and hepatic vessels using small animal imaging modalities. We analysed micro-CT images of the murine liver by integrating additional information from the published literature to develop comprehensive illustrations of the macroscopic anatomical features of the murine liver and hepatic vasculature. As a result, we provide updated three-dimensional illustrations of the macroscopic anatomy of the murine liver and hepatic vessels using micro-CT. The information presented here provides researchers working in the field of experimental liver disease with a comprehensive, easily accessible overview of the macroscopic anatomy of the murine liver.

Citation: Fiebig T, Boll H, Figueiredo G, Kerl HU, Nittka S, et al. (2012) Three-Dimensional *In Vivo* Imaging of the Murine Liver: A Micro-Computed Tomography-Based Anatomical Study. PLoS ONE 7(2): e31179. doi:10.1371/journal.pone.0031179

Editor: Simon Afford, University of Birmingham, United Kingdom

Received: November 14, 2011; **Accepted:** January 4, 2012; **Published:** February 8, 2012

Copyright: © 2012 Fiebig et al. This is an open-access article distributed under the terms of the Creative Commons Attribution License, which permits unrestricted use, distribution, and reproduction in any medium, provided the original author and source are credited.

Funding: The acquisition of the micro-CT (Yxlon Y. Fox) was funded by the Federal Ministry of Education and Research and the Land Baden-Württemberg (HBFGR grant # 125-648). The funders had no role in study design, data collection and analysis, decision to publish, or preparation of the manuscript.

Competing Interests: The authors have declared that no competing interests exist.

* E-mail: brockmann@gmx.de

Introduction

Within the last twenty years the number of publications describing the use of mouse models has steadily increased. Animal models of human disease have become an integral part of virtually all areas of medical research. Consequently, various murine models of liver disease have been developed including models of inflammatory liver disease [1,2], alcoholism [3,4], portal hypertension [5,6], parasitic infectious disease [7,8], hepatectomy [9], as well as liver tumors and metastases [10,11,12,13]. Most of these models are used for longitudinal monitoring of the disease process and to assess the effectiveness of novel therapeutic approaches. Methods that allow non-invasive longitudinal liver imaging include micro-computed tomography (micro-CT) [14,15], magnetic resonance imaging (MRI) [16], ultrasound [17], as well as more sensitive techniques with lower resolutions, such as positron emission tomography (PET) [18,19,20] and fluorescence imaging [18]. The increased availability of high-resolution imaging modalities allow researchers the opportunity (and sometimes the need) to identify with precision the pathological processes at work, making knowledge of the macroscopic anatomical situation of the murine liver essential.

To gain a better understanding of the macroscopic anatomy of the murine liver and its associated microvasculature we compiled information from our own previous research in C57BL/6 mice using micro-CT and compared our observations to the literature.

Materials and Methods

Micro-CT

Micro-CT images were acquired as described recently [14,21] using an industrial X-ray inspection system (Y.Fox; Yxlon International GmbH, Hannover, Germany) equipped with a transmission X-ray tube and a 12-bit direct digital flat bed detector (Varian PaxScan 2520; Varian, Palo Alto, CA, USA). The data used in our study was based upon previously performed liver imaging in ten male and female, 12–24 week old C57BL/6 mice with a body weight between 30–35 g. After injection of a liver specific nanoparticulate contrast agent (ViscoverTM ExiTronTM nano; Miltenyi Biotec, Bergisch-Gladbach, Germany) or a blood pool contrast agent (Fenestra VC; Advanced Research Technologies Inc., Montréal, Canada), mice were anaesthetized, intubated and imaging of the vascular structures and of the liver was performed using the following scan parameters: tube current 80 kV; 75 μ A; 190° rotation within 40 sec scan time and continuous image acquisition at 30 fps (frames per second). The resulting 1200 projections were reconstructed using the software provided by the manufacturer (Recon Studio; Yxlon International GmbH) using a filtered back projection algorithm with a matrix of 512×512×512. The voxel size ranged between 39×39×52 μ m and 41×41×55 μ m. Coronal, sagittal, and axial reconstruction were prepared. All experiments were carried out after receiving the local ethics committee approval (Regierungspräsidium Karlsruhe; G-202/10). Institutional guidelines for animal welfare and experimental conduct were followed.

Literature search analysis

Our literature search utilized, the search engines Medline, Google, and Vetseek [22], and also included veterinary anatomy books [23,24,25,26,27]. The search terms included: anatomy, mouse, mice, murine, liver, hepatic, hepatectomy, and imaging. To create comprehensive up-to-date illustrations of the murine liver, our review focused on gathering information that specifically detailed the shape, fixation and impressions of the liver, the location of the lobes, the adjacent perihepatic organs and the liver-related vessels.

Results

Literature search

Searching Medline we found four articles describing the macroscopic anatomy of the murine liver [9,28,29,30]. In these four articles, three different terminologies for the anatomical description of the liver lobes were used and none of the descriptions conformed with *Nomina Anatomica Veterinaria* (NAV) which is the standard reference in veterinary science for anatomical terminology [31].

In addition to the journal articles available online, we identified seven books that included a description of the murine liver anatomy [23,24,25,26,27,32]. Within the seven books, five different terminologies were used for the anatomical description of the liver. While four books did not refer to the NAV at all [23,24,25,33], three books [26,27,32] used a simplified version of the of the NAV.

During our literature search we found no articles or books that comprehensively reviewed the murine liver anatomy with regard to the classical slice orientations used in small animal in vivo-imaging, nor did we find any articles that described the adjacent liver vessels in this context.

Anatomy of the murine liver

Shape and impressions of the liver. The murine liver has a convex shaped cranial surface conforming to the vault of the diaphragm and a concave shaped caudal surface, which is adapted to the surface of the abdominal organs. While the gastric impression (*Impressio gastrica*) of the caudal surface of the left lateral liver lobe is caused by the stomach, the right kidney lies

within the renal impression (*Impressio renalis*) located on the caudal surface of the caudate lobe. Other impressions of the liver are the duodenal (*Impressio duodenalis*), oesophageal (*Impressio esophagea*), and the jejunal impression (*Impressio jejunalis*), which are difficult to identify in small animal imaging.

Ligaments. The liver is fixed in place by several ligaments. On the dorsal surface the left medial liver lobe and the left lateral liver lobe are fixed to the diaphragm by the coronary ligament (*Ligamentum coronarium*) and the triangular ligament (*Ligamentum triangulare sinistrum*), respectively. According to the literature, mice have no ligaments stabilizing the right medial and right lateral liver lobe. On the right side, only the caudate process is fixed to the right kidney by the hepatorenal ligament (*Ligamentum hepatorenale*). Ventrally, the falciforme ligament (*Ligamentum falciforme*) containing the teres ligament (*Ligamentum teres hepatis*), is considered a relic of embryonic development rather than a ligament of fixation (Figure 1B and 1C).

Anatomy of the liver lobes. According to the NAV, the liver is divided into four lobes that can be further subdivided, as schematically illustrated in Figure 1A, the following photographs (Figures 1B, 1C), and the reconstructions of micro-CT imaging in Figures 2, 3, 4.

The left liver lobe can be divided into the left medial lobe (yellow color-coding) and the left lateral lobe (red color-coding), with the smaller left medial lobe lying cranially and medially to the larger left lateral lobe (Figures 1, 2, 3, 4).

Similarly, the right liver lobe can be subdivided into the right medial lobe (blue color-coding), which is located directly below the diaphragm and lateral to the right side of the gall bladder, and the right lateral lobe (green color-coding), which is smaller and located more caudally than the right medial lobe.

The caudate lobe is subdivided into the larger caudate process (cyan color-coding) and the smaller papillary process (magenta color-coding). The larger caudate process lies directly caudal to the right lateral lobe and overlaps the right kidney ventrally and laterally. The papillary process in general is relatively small, and can be subdivided into two smaller parts (no specific nomenclature exists for these two subdivided parts) and is located between the stomach, the right lateral lobe, and the caudal caval vein.

Finally, the quadrate lobe is described in the NAV. This lobe is located at the medial edge of the left lateral lobe and is not further subdivided. While we have not been able to identify this small lobe

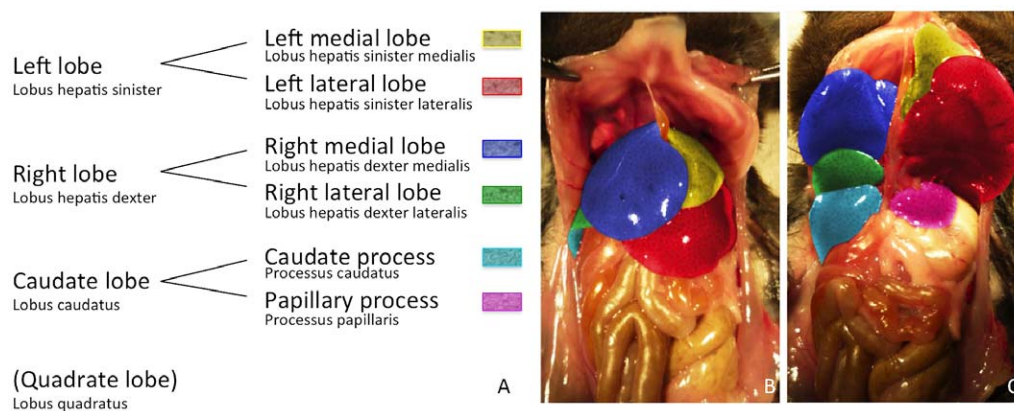


Figure 1. Illustrating the segmentation of the murine liver lobes according to the *Nomina Anatomica Veterinaria*. **A** Since in most animals we have not been able to identify the quadrate lobe in micro-CT imaging or in situ, the quadrate lobe was put in brackets and not color-coded. **B** and **C** are photographs of the liver of a C57BL/6J mouse (ventral view). In **C** the left and the right liver lobe have been folded cranially to reveal the liver lobes lying below. The single liver lobes have been consistently color-coded according to the schematic segmentation (**1A**) and to the related micro-CT figures 2, 3, 4 to simplify orientation.

doi:10.1371/journal.pone.0031179.g001

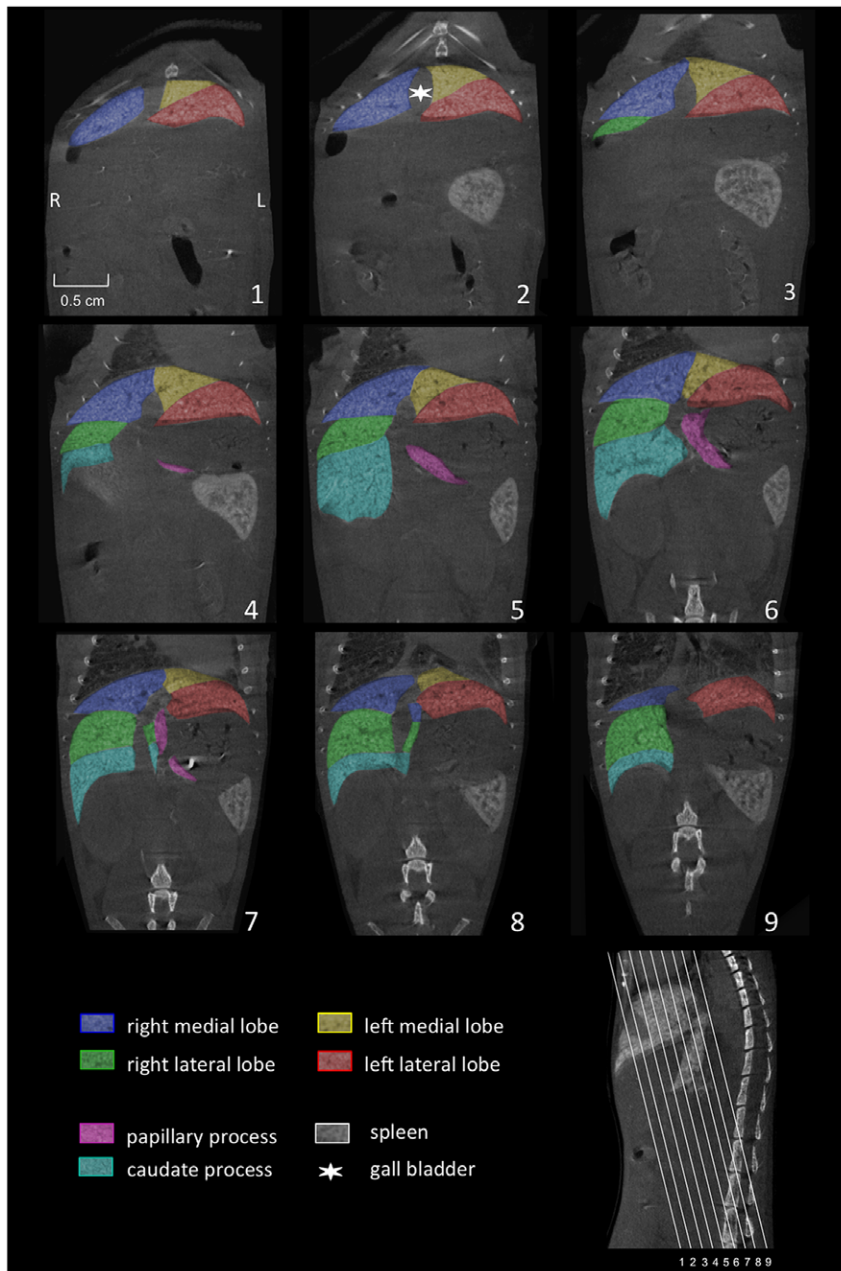


Figure 2. Coronally reconstructed micro-CT images. Imaging of the liver of a C57BL/6J mouse was performed 3 hours after i.v. injection of 100 μ l of a nanoparticulate contrast agent (ExiTron nano 12000). The color-coding of the single liver lobes corresponds to the color coding presented in Figure 1. The slice orientation in relation to the spine is shown in the lower right corner. doi:10.1371/journal.pone.0031179.g002

of the liver macroscopically or with micro-CT images, other authors depicted the quadrate lobe in their schematic drawings without labeling it within the images [26,32]. Only Popeskow et al. [27] correctly depicted and labeled the quadrate lobe in their schematic drawing. Although very small in mice, the quadrate lobe has been described as an independent lobe in the NAV, mainly because in many other animals the lobe is larger and therefore more easy to identify.

Anatomical variations. While anatomical variations of the liver do exist both within and between different mouse strains, to date, we did not evaluate these differences in-depth. However, we observed variations in our own measurements at the fusion of the

two middle lobes. This variation has been described, by Rauch et al. [34] as fission rather than of fusion of the lobes especially among male animals. Other noted variations include the shape and size of the single liver lobes. Figure 5A–C illustrates the variability of the size of the papillary process.

Perihepatic structures and hepatic vessels

To compliment the anatomical description of the liver we also gathered additional information on the anatomical relations of the adjacent perihepatic organs and liver-related vessels.

Organs adjacent to the liver. Only separated by the diaphragm, the heart and the lungs are cranial to the liver.

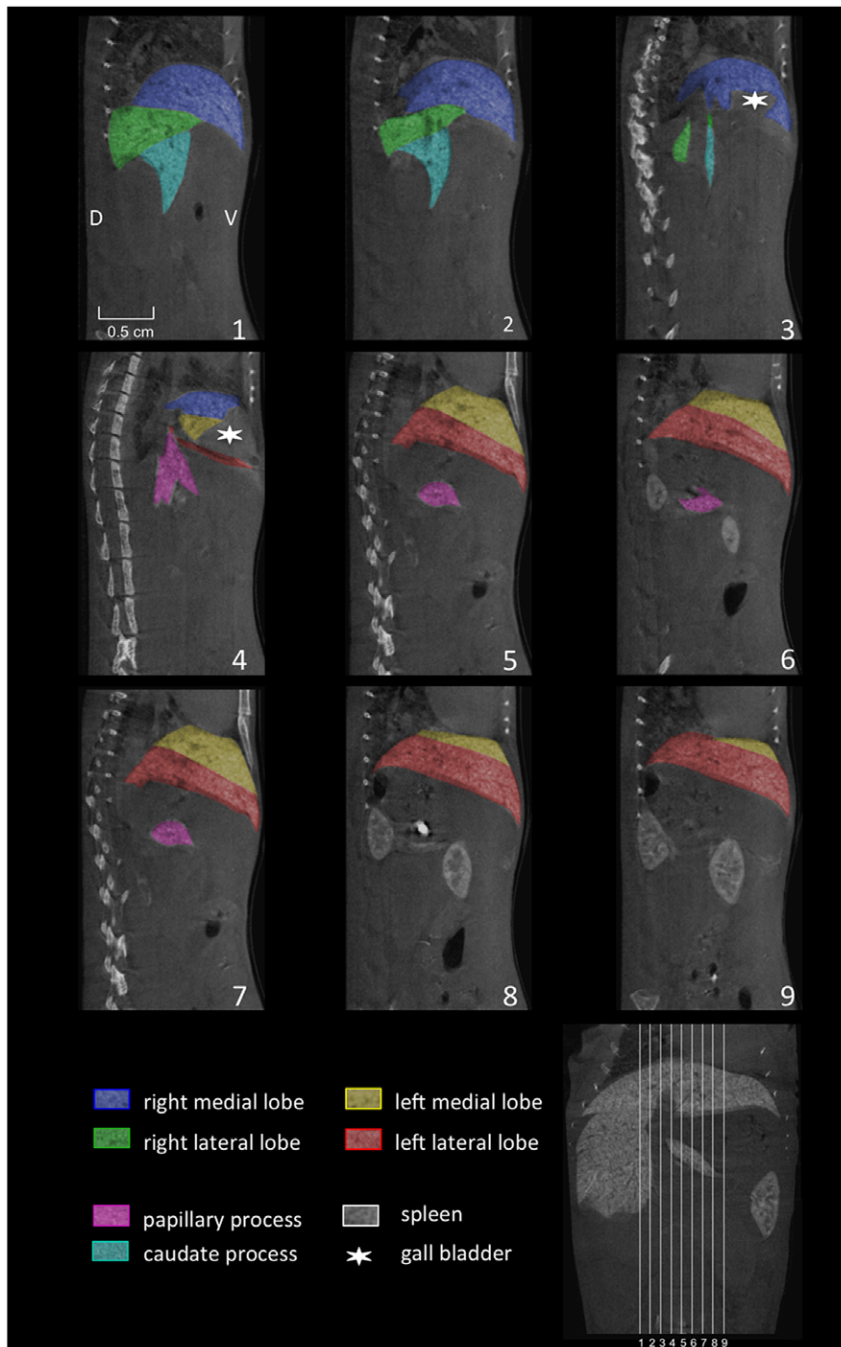


Figure 3. Sagittal reconstructed micro-CT images. Micro-CT of the liver of a C57BL/6J mouse was performed 3 hours after injection of 100 μ l of a nanoparticulate contrast agent (ExiTron nano 12000). The color-coding of the single liver lobes corresponds to the color coding presented in Figure 1. The slice orientation in relation to a coronal section is shown in the lower right corner. doi:10.1371/journal.pone.0031179.g003

While these organs are often easily distinguished from the liver, in one case we observed transdiaphragmatic herniation of the right medial liver lobe, which was clearly identifiable just after administration of a liver-specific contrast agent (Figure 5D).

The half-moon shaped spleen can be found caudal to the liver, kidneys, adrenal glands, and stomach (Figure 6D). As mentioned earlier in the manuscript, the right kidney lies a little more cranially towards the left kidney, reaches the liver surface and lies within the renal impression (*Impressio renalis*) of the liver. Between the medial cranial pole of the kidneys and

the liver the triangularly shaped adrenal glands are located on both sides (Figure 6D). On the left side of the abdomen the stomach lies within the gastric impression (*Impressio gastrica*) adjacent to the surface of the left lateral lobe, while the spleen is located between the left kidney, the stomach, and left abdominal wall.

Hepatic artery. The coeliac artery (*Arteria coeliaca*; Figure 6C) arises from the abdominal aorta before the cranial mesenteric artery (*A. mesenterica cranialis*, in humans the superior mesenteric artery) and among others branches into the hepatic artery which

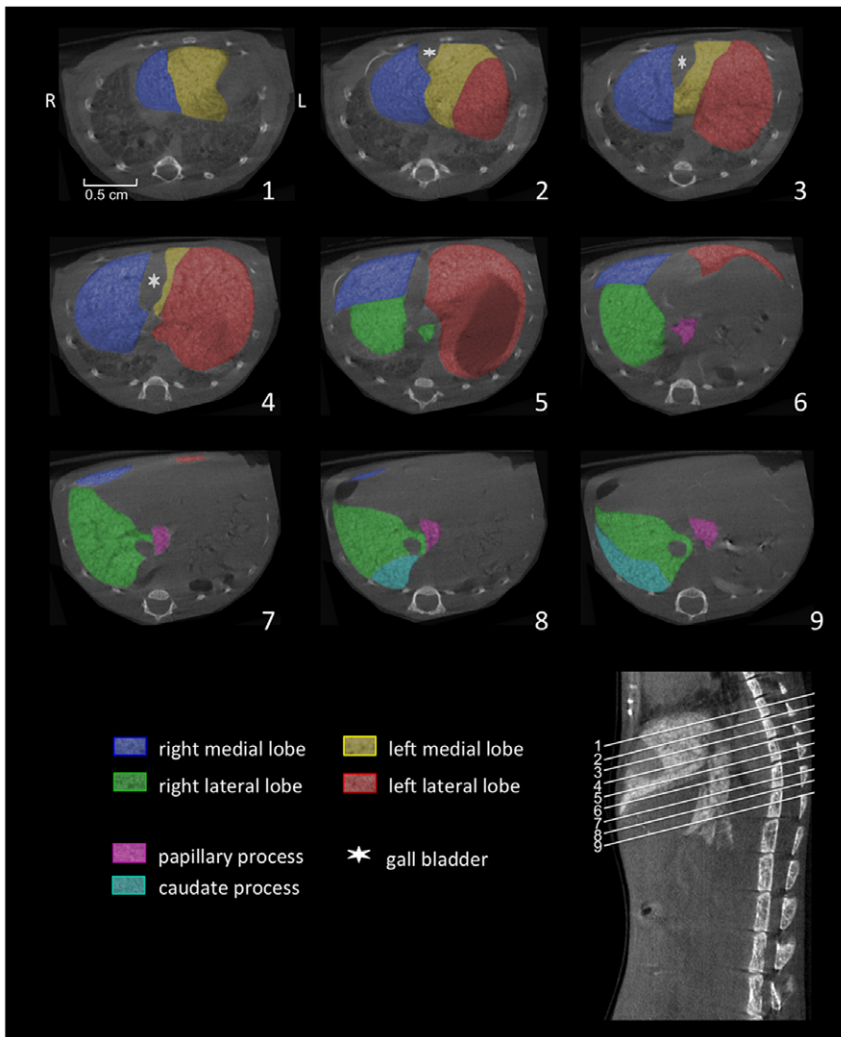


Figure 4. Axial reconstructed micro-CT images. Micro-CT of the liver of a C57BL/6J mouse was performed 3 hours after injection of a nanoparticulate contrast agent (ExiTron nano). The color-coding of the single liver lobes corresponds to the color coding presented in Figure 1. The orientation of the axial slices in relation to the spine is shown in the lower right corner. doi:10.1371/journal.pone.0031179.g004

runs cranially. Due to the limitations of in vivo micro-CT of the hepatic artery we have been able to identify the proximal hepatic artery, but cannot trace this vessel into the liver. However, the

branching pattern of the hepatic artery has been reported to correspond with the branching of the portal vein and the biliary ducts [35,36].

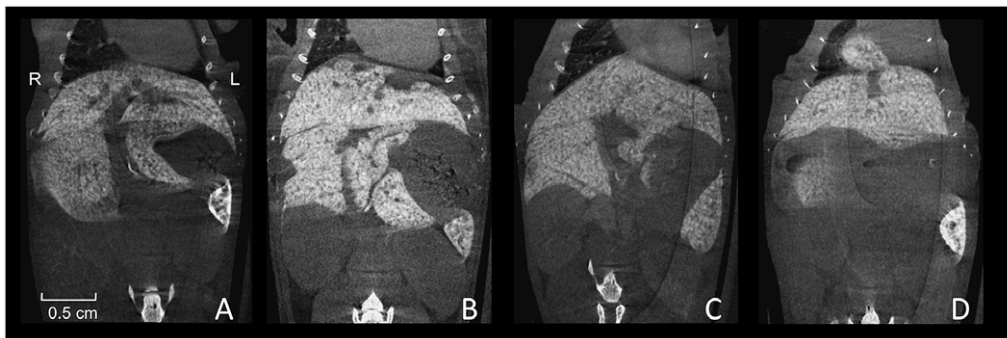


Figure 5. Liver variations. A–C are comparable coronal sections of the murine liver illustrating the variability of the size of the papillary process of the caudate lobe. D shows transdiaphragmatic herniation of parts of the right medial liver lobe, which we incidentally discovered during our studies. doi:10.1371/journal.pone.0031179.g005

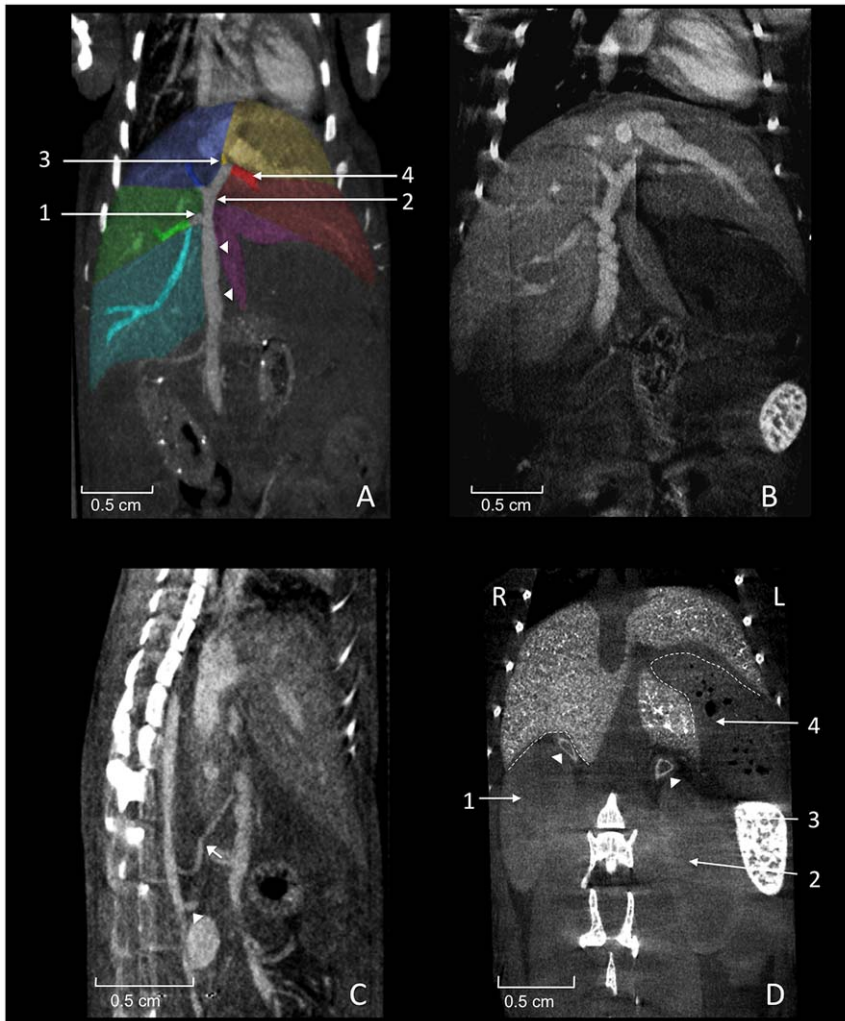


Figure 6. Perihepatic structures. **A** shows coronally reconstructed micro-CT images acquired 20 minutes after injection of 400 μ l Fenestra VC. The portal vein (arrowheads) runs in a caudocranial direction and divides into single veins supplying the liver lobes with blood from the abdominal organs. The right branch (1; *Ramus dexter*) divides up into two non-specified branches supplying the right lateral lobe (colored green) and the right caudate process (colored cyan). The left branch (2; *Ramus sinister*) divides into the umbilical part (3; *Pars umbilicalis*) and the transversal part (4; *Pars transversalis*) draining the left medial lobe and the left lateral lobe, respectively. The vein supplying the right medial liver lobe (colored blue) is not classified in the NAV. Spontaneous peristaltic movement of the portal vein is known to result in a corkscrew-like appearance of the vessel as shown in **B**. The liver is supplied with arterial blood from the coeliac artery (arrow) arising from the aorta cranial of the cranial mesenteric artery (arrowhead), as shown in **C**. The portal vein collecting blood from smaller abdominal vessels can be spotted directly ventral to the hepatic artery. **D** shows a coronally reconstructed micro-CT, 21 days after injection of 100 μ l Exitron nano 12000 showing relevant organs adjacent to the liver. The right kidney (1), the left kidney (2), the spleen (3), the stomach (4; containing air bubbles), and the adrenal glands (arrow heads). The dotted lines indicate the renal impression of the liver on the right side and the gastric impression on the left side.
doi:10.1371/journal.pone.0031179.g006

Portal vein. The portal vein drains blood from the gastrointestinal tract and spleen to the liver. The portal vein divides into the right branch (*Ramus dexter*) draining into the caudate process and the right lateral lobe (Figure 6A), and the left branch (*Ramus sinister*). The left branch provides blood-flow into the right medial lobe and divides into the umbilical part (*Pars umbilicalis*) for the left medial lobe and the transversal part (*Pars transversalis*) for the left lateral lobe. The NAV provides no specific nomenclature for the small branch providing blood supply to the papillary process.

Hepatic veins. The hepatic veins are not well described in the NAV. Only a left, a right, and a medial hepatic vein are described. However, using in vivo micro-CT angiography, more veins draining into the inferior vena cava can be identified (Figure 7). To address this

problem we referred to the NAV to describe the side of the vein, and added information on the draining territory (i.e. lateral or medial), which matches the nomenclature of the right and the left liver lobe. For the processes of the caudate lobe we extended the name of the vein by adding the name of the drained lobe (i.e. the left papillary hepatic vein).

The most caudally located vein draining the caudate process is the right caudate hepatic vein. The next most cranially located branch on the right side draining the right medial lobe is the right medial hepatic vein, while the right lateral lobe is drained by the right lateral hepatic vein.

The left lateral liver lobe is drained by the left lateral hepatic vein. The left medial lobe is drained by the left medial hepatic vein, that drains into the left lateral hepatic vein. The papillary

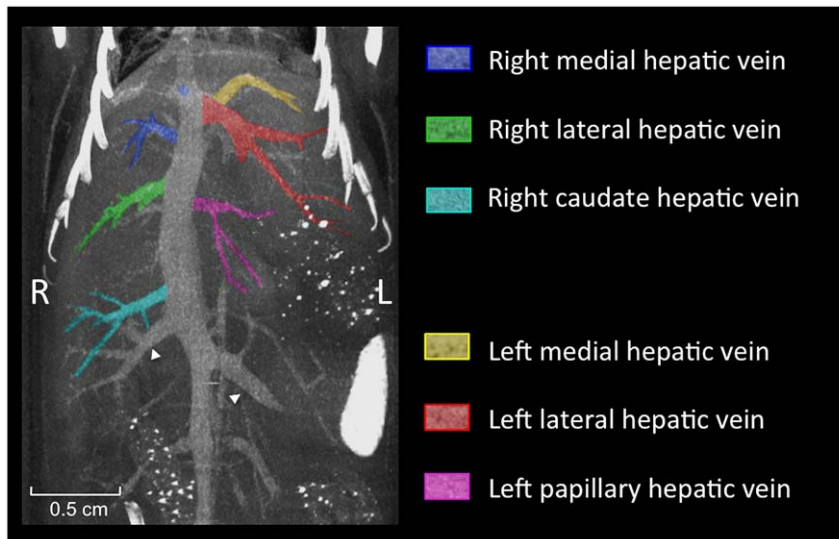


Figure 7. Hepatic veins. Maximum intensity projection (MIP) of micro-CT images of the murine hepatic veins 20 minutes after injection of 400 μ l Fenestra VC. The color coding of the draining veins corresponds to the color coding used for the liver lobes before. The renal veins are indicated by arrowheads.

doi:10.1371/journal.pone.0031179.g007

process of the caudate lobe is drained by a small, separate branch which would be termed the left papillary hepatic vein.

Biliary tract

Using contrast agents that are not being excreted via the biliary tract, the only clearly identifiable part of the biliary system in micro-CT images is the gall bladder, which is depicted in Figures 2, 3, 4.

Discussion

Searching the literature we found a limited number of publications sparsely describing the macroscopic anatomy of the murine liver [23,24,25,26,27,30]. In addition, we found no existing publications referring to the increasingly available imaging modalities. Within the publications that described the macroscopic anatomy of the murine liver we noted a lack of consistency in nomenclature [30,35]. Reasons for the inconsistency in terminology includes the alternating use of Latin and English terminology and, more problematic, inconsistency in nomenclature of the structures between different authors [9,24,26,27,37]. For example, while the left liver lobe (according to the NAV) was correctly divided into the left lateral and left medial liver lobe by Popesko et al. [27], other authors divided the left liver lobe into the left lateral lobe and the left part of the medial lobe [24,25,28,30]. Likewise, the lobes of the right side of the murine liver have been found to be accompanied by different adjectives including “posterior”, “anterior”, “inferior”, “superior”, “upper” and “lower” by different authors [9,24,28,30,35,37,38], again creating confusion.

The most serious differences exist in the terminology of the quadrate lobe and the caudate lobe (with the latter one according to the NAV being subdivided into the papillary process and the caudate process). For example, some authors described the caudate process (of the caudate lobe) as the caudate lobe [26,27] or the right lower lobe [9], while other authors named the papillary process as the caudate [23,24,25,28,30] or the omental lobe [9], due to its anatomical surroundings.

To overcome the problems that may arise from the inconsistent designation of the liver lobes we recommend using the

nomenclature in accordance with the *Nomina Anatomica Veterinaria*, which was introduced in 1955 and since then has continuously been updated by an international group of veterinarians. Regarding the murine liver lobes we found the NAV to serve almost perfectly (with the only exception that we found it difficult to identify the quadrate lobe). However, there were some problems in the most recent edition of the NAV from 2005 [31]. For example, as noted in the results section, the nomenclature of the draining veins of the liver, as described in the NAV, are not easily transferrable to mice.

Photographs and schematic drawings are primarily used in virtually all other publications dealing with the anatomy of the murine liver. Although different three-dimensional mouse atlases are available in book form [23,27,33] and online [39,40], the precision of the anatomical description of the liver isn't as comprehensive as presented here. To better represent the increasing use of small animal imaging modalities in liver research, we present the anatomy of the murine liver using the three typical radiological cut planes implemented in tomographic imaging which allows for a faster and better orientation of the liver relative to other adjacent anatomical structures. This might be helpful for anatomical studies or to reveal strain differences, but also for animal models of human disease as described in the introductory section and as exemplarily shown in figure 8.

While our study aimed at providing a general overview of the macroscopic anatomy of the murine liver, we did not investigate differences related to mouse strain, gender, weight, or age. These differences, however, have to be considered when trying to refer to the anatomical descriptions presented in our manuscript.

Conclusion

The provided three-dimensional illustrations of the macroscopic anatomy of the murine liver using micro-CT may promote clarity and precision among scientists and veterinarians working in the field of liver research and may be helpful as a reference for future experimental research in this field.



Figure 8. Illustrative micro-CT images of liver metastases in a mouse. A–C Images of liver metastases were acquired 2 hours after i.v. injection of 100 μ l of a contrast agent (Viscoveer Exitron nano 6000; Miltenyi Biotec, Bergisch-Gladbach, Germany) in a coronal (A), transversal (B), and saggital (C) slice orientation. With regard to liver anatomy, we found metastases to develop predominantly under the liver capsule adjacent to the fissures between the liver lobes. While the left lateral lobe (LLL) shows no metastases on its caudal edge in this slice, there are plenty on its cranial edge, next to the left medial lobe (LML). The lobes on the right side (right medial lobe (RML), right lateral lobe (RLL) and the caudate process (CP)) show (besides the subcapsular growth pattern) metastases within the liver parenchyma. Due to tumor growth the papillary process depicted in B and C lost its typical shape (compare with figs. 2, 3, 4).
doi:10.1371/journal.pone.0031179.g008

Acknowledgments

We are indebted to Dr. Fabian Doyon (University of Heidelberg, Medical Faculty Mannheim, Department of Surgery) for technical assistance with the murine model of liver metastasis.

References

- Dorner M, Horwitz JA, Robbins JB, Barry WT, Feng Q, et al. (2011) A genetically humanized mouse model for hepatitis C virus infection. *Nature* 474: 208–211.
- Kuhara T, Yamauchi K, Iwatsuki K (2011) Bovine lactoferrin induces interleukin-11 production in a hepatitis mouse model and human intestinal myofibroblasts. *Eur J Nutr*; in press.
- Gabele E, Dostert K, Dorn C, Patsenker E, Stickel F, et al. (2011) A new model of interactive effects of alcohol and high-fat diet on hepatic fibrosis. *Alcohol Clin Exp Res* 35: 1361–1367.
- Yan AW, Fouts DE, Brandl J, Starkel P, Torralba M, et al. (2011) Enteric dysbiosis associated with a mouse model of alcoholic liver disease. *Hepatology* 53: 96–105.
- Van Steenkiste C, Staelens S, Deleye S, De Vos F, Vandenberghe S, et al. (2010) Measurement of porto-systemic shunting in mice by novel three-dimensional micro-single photon emission computed tomography imaging enabling longitudinal follow-up. *Liver International* 30: 1211–1220.
- May D, Djonov V, Zamir G, Bala M, Safadi R, et al. (2011) A Transgenic Model for Conditional Induction and Rescue of Portal Hypertension Reveals a Role of VEGF-Mediated Regulation of Sinusoidal Fenestrations. *PLoS one* 6: e21478.
- Duan YN, Qian HY, Qin YW, Zhu DD, He XX, et al. (2011) Dynamics of Sept4 expression in fibrotic livers of mice infected with *Schistosoma japonicum*. *Parasitology* 138: 1003–1010.
- Kolbekova P, Kolarova L, Vetvicka D, Syrucek M (2011) Imaging of *Toxocara canis* larvae labelled by CFSE in BALB/c mice. *Parasitol Res* 108: 1007–1014.
- Greene AK, Puder M (2003) Partial hepatectomy in the mouse: technique and perioperative management. *J Invest Surg* 16: 99–102.
- Martiniova L, Schimel D, Lai EW, Limpuangthip A, Kvetnansky R, et al. (2010) In vivo micro-CT imaging of liver lesions in small animal models. *Methods* 50: 20–25.
- Almajdub M, Nejjari M, Poncet G, Magnier L, Chereul E, et al. (2007) In-vivo high-resolution X-ray microtomography for liver and spleen tumor assessment in mice. *Contrast Media Mol Imaging* 2: 88–93.
- Graham KC, Detombe SA, MacKenzie LT, Holdsworth DW, MacDonald IC, et al. (2008) Contrast-enhanced microcomputed tomography using intraperitoneal contrast injection for the assessment of tumor-burden in liver metastasis models. *Invest Radiol* 43: 488–495.
- Jensen MR, Factor VM, Fantozzi A, Helin K, Huh CG, et al. (2003) Reduced hepatic tumor incidence in cyclin G1-deficient mice. *Hepatology* 37: 862–870.
- Boll H, Bag S, Schambach SJ, Doyon F, Nitka S, et al. (2010) High-speed single-breath-hold micro-computed tomography of thoracic and abdominal structures in mice using a simplified method for intubation. *J Comput Assist Tomogr* 34: 783–790.
- Schambach SJ, Bag S, Schilling L, Groden C, Brockmann MA (2010) Application of micro-CT in small animal imaging. *Methods* 50: 2–13.
- Inderbitzin D, Stoupis C, Sidler D, Gass M, Candinas D (2007) Abdominal magnetic resonance imaging in small rodents using a clinical 1.5 T MR scanner. *Methods* 43: 46–53.
- Fernandez-Dominguez I, Echevarria-Uraga JJ, Gomez N, Luka Z, Wagner C, et al. (2011) High-frequency ultrasound imaging for longitudinal evaluation of non-alcoholic fatty liver disease progression in mice. *Ultrasound Med Biol* 37: 1161–1169.
- Kagadis GC, Loudos G, Katsanos K, Langer SG, Nikiforidis GC (2010) In vivo small animal imaging: current status and future prospects. *Med Phys* 37: 6421–6442.
- Loudos G, Kagadis GC, Psimadas D (2011) Current status and future perspectives of in vivo small animal imaging using radiolabeled nanoparticles. *Eur J Radiol* 78: 287–295.
- Hutchins GD, Miller MA, Soon VC, Receveur T (2008) Small animal PET imaging. *ILAR J* 49: 54–65.
- Boll H, Nitka S, Doyon F, Neumaier M, Marx A, et al. (2011) Micro-CT based experimental liver imaging using a nanoparticulate contrast agent: a longitudinal study in mice. *PLoS One* 6: e25692.
- Berlin FU (2011) Available: <http://www.vetseek.info>. Fachbereich Veterinärmedizin der Freien Universität Berlin.
- Hummel KP, Richardson FL, Fekete E (1966) *Anatomy In: Green EL, ed. Biology of the Laboratory Mouse*. 2 ed. New York: Dover Publications, Inc.
- Maronpot RR (1999) *Pathology of the Mouse*. Vienna: Cache River Press. pp 120–122.
- Cook MJ (1965) *The Anatomy of the Laboratory Mouse*. London: Academic Press.
- Hedrich H, Bullock GR (2004) *The Laboratory Mouse*. Oxford: Elsevier Academic Press. pp 117–132.

27. Popesko P, Rajtova V, Horak J, Kosice P (1992) *Colour Atlas of Anatomy of Small Laboratory Animals*. London: Wolfe Publishing Ltd. pp 107–166.
28. Martins PN, Theruvath TP, Neuhaus P (2008) Rodent models of partial hepatectomies. *Liver Int* 28: 3–11.
29. Studer P, Sidler D, Gloor B, Dutly AE, Candinas D, et al. (2005) Basics of mouse liver anatomy from a microsurgical point of view. *Gastroenterology* 134: A875–876.
30. Hollander CF, van Bezooijen CF, Solleveld HA (1987) Anatomy, function and aging in the mouse liver. *Arch Toxicol* 10: 244–250.
31. Nomenclature ICoVGA (2005) *Nomina Anatomica Veterinaria*: Editorial Committee Hannover, Colubia, Gent, Sapporo.
32. Fox JG (2007) *The Mouse in Biomedical Research*. Oxford: Elsevier. pp 1–22.
33. Takamasa I, Hiroshi Y, Toshiyuki H (2001) *A Color atlas of sectional anatomy of the mouse*. Tokyo: Adthree Publishing.
34. Rauch H (1952) Strain differences in liver patterns in mice. *Genetics* 37: 617.
35. Martins PN, Neuhaus P (2007) Surgical anatomy of the liver, hepatic vasculature and bile ducts in the rat. *Liver Int* 27: 384–392.
36. Kline TL, Zamir M, Ritman EL (2011) Relating Function to Branching Geometry: A Micro-CT Study of the Hepatic Artery, Portal Vein, and Biliary Tree. *Cells Tissues Organs* 194: 431–442.
37. Madrahimov N, Dirsch O, Broelsch C, Dahmen U (2006) Marginal hepatectomy in the rat: from anatomy to surgery. *Ann Surg* 244: 89–98.
38. Kogure K, Ishizaki M, Nemoto M, Kuwano H, Makuuchi M (1999) A comparative study of the anatomy of rat and human livers. *J Hepatobiliary Pancreat Surg* 6: 171–175.
39. Dogdas B, Stout D, Chatziioannou AF, Leahy RM (2007) Digimouse: a 3D whole body mouse atlas from CT and cryosection data. *Phys Med Biol* 52: 577–587.
40. Galvez J (2011) The visible mouse project. Available: <http://tvmouse.compmc.ucdavis.edu/>.